Organic & Biomolecular Chemistry

ROYAL SOCIETY OF CHEMISTRY

PAPER

View Article Online
View Journal | View Issue

Cite this: Org. Biomol. Chem., 2026, 24, 1120

Supramolecular light-switchable triazole-hosts for photoresponsive anion binding

Leon Hoppmann,†[a] Leonard Wyszynski, †[b] Marcus Böckmann,[c] Pascal Steinforth, [b] Lukas-Maximilian Entgelmeier,[a] Nikos Doltsinis, [c] Olga García Mancheño *[a,d] and Monika Schönhoff *[b]

Received 22nd October 2025,
Accepted 9th January 2026

DOI: 10.1039/d5ob01664a

rsc.li/obc

A series of photoreversible anion binding hosts is developed, combining either an azobenzene or an arylazopyrazole as a central photoswitch unit and tetrakis-triazoles as anion binding motifs. By broad structural variations, including different linker types and positions between the triazoles, the anion binding contrast of both isomers is maximized, with the *Z* isomer exhibiting a binding constant of up to a factor of 16 larger than that of the *E* isomer. Back-isomerisation $Z \rightarrow E$ is studied with respect to the influence of a bound anion. Anion binding stabilizes the *Z*-isomer against thermal isomerization, providing a two-fold lifetime of the *Z* isomer. A reduced photoisomerization rate and an enhanced *Z*/*E* ratio in the photostationary state correlate with the anion binding constant of the *Z* isomer, which is probably due to the modified photophysical processes.

Introduction

The field of anion recognition using synthetic supramolecular receptors[1,2] able to recognize or respond to negatively charged species through non-covalent interactions such as hydrogen bonding (HB) is gaining increasing attention, allowing for a broad application spectrum in sensing,[3] anion waste separation,[2,4] transmembrane transport,[5] and catalysis.[6]

An interesting approach for supramolecular anion recognition is the development of switchable anion binding host systems to afford modulation of ion binding and release by switching between strongly and weakly binding states.[7–9]

Due to its simple and localized applicability, light is a very versatile trigger, and correspondingly photoswitchable supramolecular hosts have recently gained attraction.[10] Since the early work of Shinkai, Manabe and co-workers on potassium receptors,[11] the field of photoresponsive cation hosts has become well established.[8] Complementarily, photoswitchable hosts for anions have also been designed later,[9] aiming at extending their application to anionic guests.[8,9] Anion binding hosts are attractive components for many applications, as they may control ionic strength and allow triggered release of anions, as ion availability is a relevant factor in physiological, chemical and technological processes.[12] To this end, several structural motifs combining photoswitchable units and anion binding groups have been developed.[7,8] A remarkable achievement toward anion-tunable thermal isomerization control was reported in 2014 by the group of Jurczak with an urea-appended azobenzene system, which showed distinct binding between the *E* and *Z* isomers and acceleration of the $Z \rightarrow E$ back-isomerization based on the anion concentration and binding affinity strength to the *Z*-isomer (Fig. 1a).[13] In the context of anion-tunable photoswitchable systems, the development of triazole-based photoresponsive anion receptors has been a major advancement.[14–19,20,21–24] Along these lines, several azobenzene-based photoswitchable hosts have already been demonstrated, utilizing hydrogen-,[14–18] halogen-,[21–23] or chalcogen-bonding[24] interactions mediated by triazole units (Fig. 1b). Since the initial report by Jiang and co-workers in 2010 using an azobenzole–bistriazole host,[15] which showed moderate contrast between its *E*- and *Z*-form for the binding to chloride anions, some efforts have been made to improve such systems.[16–18,21] In this regard, Hua and Flood addressed the photoisomerisation behavior of tetrakis-triazole bis-azobenzene foldamers and their binding ability towards chloride anions for ion capture/release applications (Fig. 1b).[17,21] High levels of photoreversibility were achieved when attaching two terminal azobenzene units, yielding a considerably larger binding constant for the *E*-form of both switches ($K_{E,E}$ 3000 M^{-1} in MeCN), as compared to the *Z*,*Z*-form (8-fold weaker),

[a]Institute of Organic Chemistry, University of Münster, Corrensstraße 36, 48149 Münster, Germany. E-mail: olga.garcia@uni-muenster.de
[b]Institute of Physical Chemistry, University of Münster, Corrensstraße 28/30, 48149 Münster, Germany. E-mail: schoenho@uni-muenster.de
[c]Institute of Solid State Theory and Center for Multiscale Theory and Computation, University of Münster, Wilhelm-Klemm-Straße 10, 48149 Münster, Germany. E-mail: nikos.doltsinis@uni-muenster.de
[d]Leibniz Institute for Catalysis e. V., Albert-Einstein-Str. 29a, Rostock, 18059, Germany. E-mail: olga.garcia@catalysis.de
† These authors contributed equally.

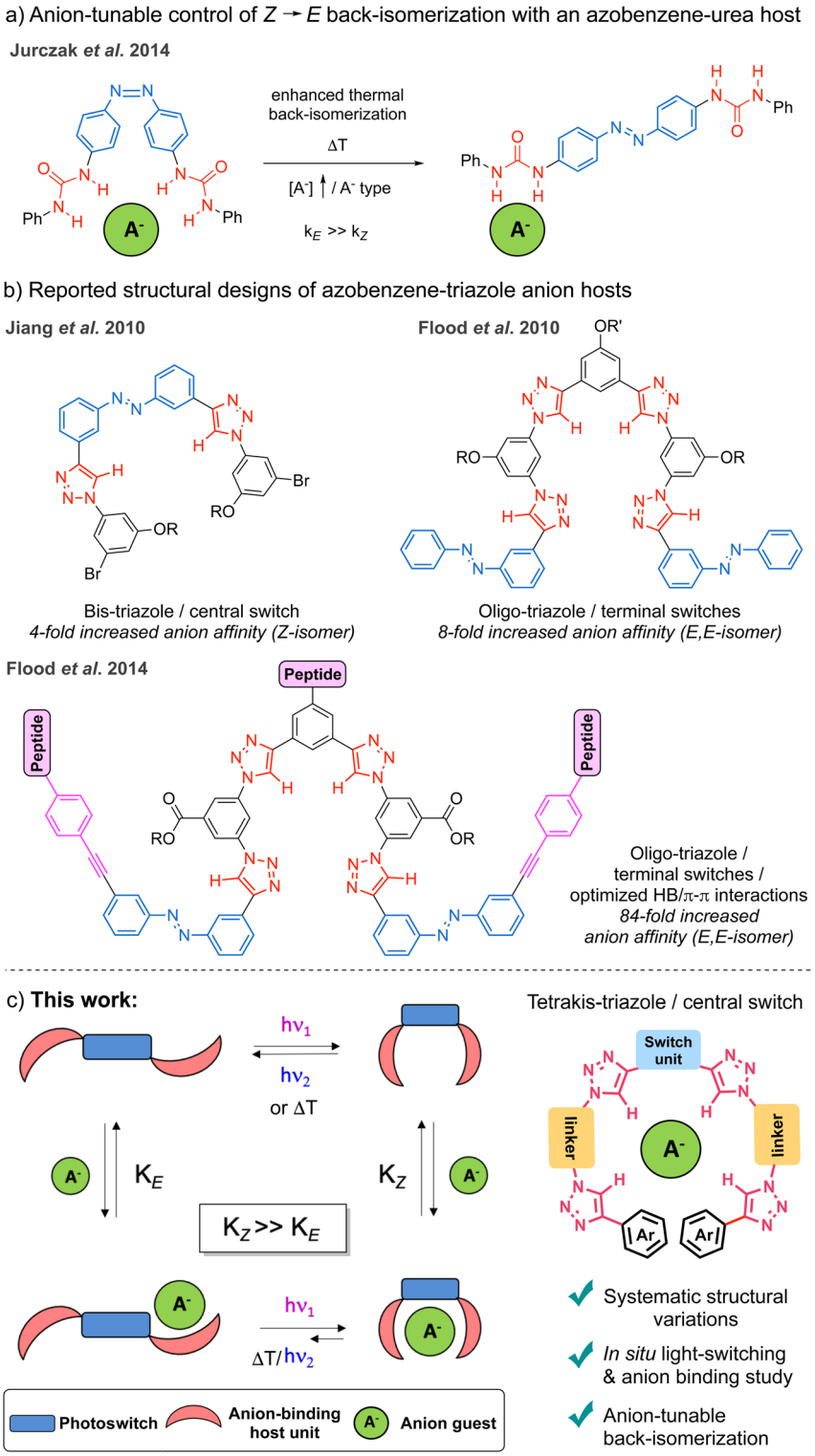

Fig. 1 (a) $Z \rightarrow E$ back-isomerization control with azobenzene–urea anion hosts. (b) Previously reported azobenzene–triazole photoswitchable anion hosts, and (c) concept of tunable photoisomerization towards the underlying anion binding status (left) and our proposed basic structure of a photoswitchable host with variable linker and switching units (right).

resulting from conformational changes.[16] This could be further improved by the introduction of β-sheet-like hydrogen bond chains in the structure, as well as alkyne units to enable additional π–π interactions, to interlock the helical turns of the photoswitchable foldamer host, thus reaching the state of the art in anion binding contrast with such systems (up to $K_{E,E}$

970.000 M^{-1} in MeCN/THF (1 : 1) and 84-fold contrast to the *Z*,*Z*-form).[18] Moreover, it is important to note that additional examples featuring adaptive photoisomerization through ionic interactions[11,13,25] or metal coordination,[26] in which the substrate binding influences the switching properties of the hosts, further demonstrate the potential of this approach.

Building on these systems, we herein aim at optimized structures of a new family of oligo-triazole-based anion hosts bearing only one central photoswitchable element, which provide a sufficiently strong binding contrast between the *E* and *Z* forms in order to allow modulation of the $Z \rightarrow E$ back-isomerization as an application in anion binding. Fig. 1c highlights the concept of the envisioned interdependency of anion binding and photoisomerization: in a reversible system with a large contrast in anion binding affinity ($K_Z \gg K_E$) concerning two photoisomeric states (*Z* and *E*), it is expected that the strongly binding *Z*-isomer undergoes conformational stabilization. Consequently, a $Z \rightarrow E$ isomerization would be less efficient compared to a guest-free host.

To develop hosts with a maximized contrast of the binding constants, we synthesize a library of host structures with varying linkers, triazole connectivity and solubility tags. In contrast to previously reported oligo-triazole-based hosts,[16–19] the photoswitch unit forms the central structural motif, with two bis-triazole frameworks attached on either side. Besides well-established azobenzene motifs, arylazopyrazoles[27] are alternatively employed. Arylazopyrazoles offer advantageous properties as photoswitches through well-separated absorption bands of *E*- and *Z*-isomers, as well as through their high thermal stability. These features make them attractive for developing photoswitchable anion hosts. Our results show that host structures based on arylazopyrazoles show a particularly beneficial anion binding contrast of the respective isomers. We further demonstrate that both classes of hosts, based on either azobenzene or arylazopyrazole, provide photochemical properties, dependent on the state of anion binding.

Results and discussion

Anion binding optimization

To investigate the hosts' switching behavior, we used an *in situ* irradiation setup to enable continuous irradiation within an NMR spectrometer (see the SI, Fig. S28). The anion binding constants (*K*) were determined using NMR titrations. For our library of structures, we took inspiration from the parent non-switchable tetradentate anion binding host **TT1a** developed by our group[28] (Fig. 3a). Besides a demonstration of the successful anion affinity of **TT1a** towards chloride,[29] a detailed analysis of the influence of salt dissociation showed the relevance of the chosen salt cation.[30] Based on **TT1a**, a family of photoswitchable tetrakis-triazole hosts was prepared following a multi-step synthesis route (Fig. 3; see the details in the SI). In order to achieve light responsive anion-binding, the hosts should include three essential structural elements (Fig. 3b): (i) a central photoswitchable unit: azobenzene (AB) or arylazopyrazole (AAP), (ii) two triazole motifs on each side able to form a strong tetradentate anion-recognition in either the *E*- or *Z*-form, and (iii) a linker between the triazoles, which also acts as a spacer to modulate the binding efficiency. The assignment of the signals to the respective isomers can be achieved by comparing the spectra recorded at room temperature and after UV irradiation (Fig. 2, SI Fig. S33–S35).

For a first binding affinity study, we chose the host **AB-mTTA-Cy** (Fig. 3c), featuring a *meta*-functionalized azobenzene central switch, a chiral 1,2-substituted cyclohexyl moiety and terminal arenes with electron-withdrawing CF_3 groups to enhance the acidity of the triazole-C–H bond. We used spherical chloride as a model anion (with tetrabutylammonium (TBA) salt as an anion source) in acetone-d_6. Different binding constants K_E and K_Z could be observed for either isomer, with the *Z*-isomer providing a higher binding constant ($\log(K_Z/M^{-1})$ = 3.1 *vs.* $\log(K_E/M^{-1})$ = 2.4) (Fig. 4). For this host, the contrast is likely attributed to the formation of a more suitable cavity in the *Z*-isomer. In comparison with the host **TT1a** with $\log(K_Z/M^{-1})$ = 2.7 for chloride,[29] it is evident that the *Z*-azobenzene backbone enhances anion binding, while the azobenzene in the *E*-form lowers it. Other anions such as trigonal carboxylates were also suitable guests, but generally led to lower binding affinities (see the data in the SI, Fig. S7 and Table S1). Thus, chloride was proved as the most favorable anion and was then used as an anion for all further studies.

Having achieved an isomer-induced contrast of the binding constants, the next step to attain a higher anion binding affinity for the *Z*-isomer and maximize its difference from the *E*-isomer involved optimizing the host structure. So far, a 1,2-

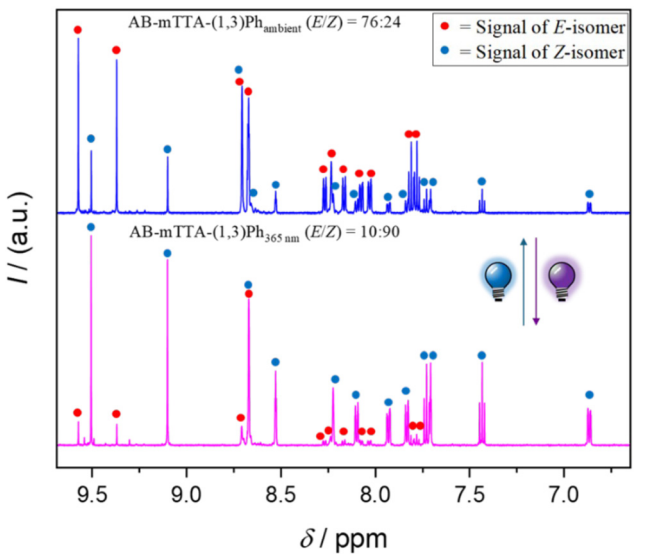

Fig. 2 ^{1}H-NMR spectra of **AB-mTTA-(1,3)Ph** (1 mM, acetone-d_6) under ambient conditions (top) and after irradiation with 365 nm UV-light (bottom) representing the distinction between signals of the *E* and *Z*-isomers, utilized as a basis for isomer-specific binding studies using NMR-titrations. For better visibility, only the spectral region of aromatic signals is shown.

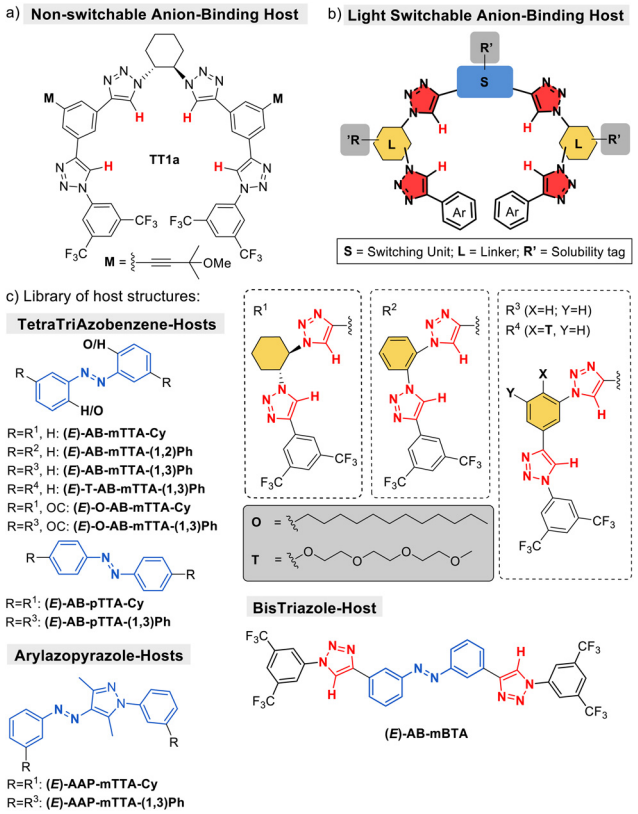

Fig. 3 (a) Host structure without photoreversibility, **TT1a**, (b) schematic depiction of a photoreversible host's structure with highlights on the different subunits, and (c) synthesized hosts with different linkers and substitutions.

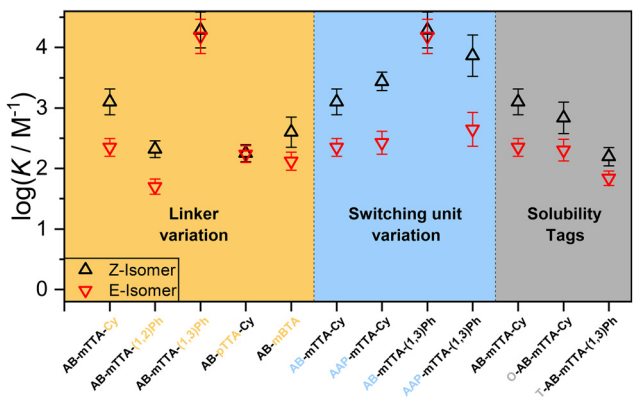

Fig. 4 Comparison of the binding constants of different hosts with chloride determined *via* NMR titration in acetone-d_6, sorted according to the structural variation.

trans cyclohexyl ring connectivity to the triazole units has been used, resulting in chiral molecules. This structural feature contributes to a host's preferred helical conformation, which in turn creates a favorable cavity for anion binding in analogy to previous hosts.[29] However, to explore the need for a chiral structure for effective anion binding, it was sought to disrupt the molecule's chirality by replacing the cyclohexyl (Cy) ring with a phenyl ring (Ph) *via* a 1,2-linkage (**AB-mTTA-(1,2)Ph**). In comparison with **AB-mTTA-Cy**, the binding strength was significantly lower (see Fig. 4). This outcome is likely due to steric hindrance, resulting in a non-coplanar conformation of the triazole protons. Further change to a 1,3-phenyl linkage (**AB-mTTA-(1,3)Ph**) should resolve the steric hindrance. Although both binding constants significantly increased, now both the *E* and *Z* configurations displayed equal binding strengths (log (K_E/M^{-1}) = 4.2 and log(K_Z/M^{-1}) = 4.3). The host molecule likely formed a large cavity in both isomers capable of binding an anion, while inefficient binding was observed for the smaller bidentate *vs.* tetradentate derivative **AB-mBTA**.

From these investigations, **AB-mTTA-Cy** and **AB-mTTA-(1,3)Ph** emerge as the most promising structures, exhibiting either significant binding contrast regarding the two isomers or very strong affinities for chloride, respectively. Compared to AB-based hosts that feature four triazole units with the switching unit located at the terminal positions (log$(K_{E,E}/M^{-1})$ = 3.5 and log$(K_{Z,Z}/M^{-1})$ = 2.6),[16] **AB-mTTA-Cy** exhibits lower binding constants. In contrast, **AB-mTTA-Ph** shows stronger overall anion binding, but with a reduced contrast between the isomers. It should also be noted that the solvents used for determining the anion binding constants differ, which limits the direct comparability.

Next, the connectivity of the azobenzene was varied from *meta* to *para*-substitution, aiming at disturbing the formation of a guest cavity in the *E*-isomer. **AB-pTTA-Cy** featured a generally lower binding strength, while also squandering all selectivity between the isomers. Unfortunately, we were unable to underline this result with the *para*-substituted analogue **AB-pTTA-(1,3)Ph** as its solubility in acetone or dichloromethane was too low for a sufficient NMR titration. The described AB-hosts follow a clear trend regarding their solubility, with planar and rigid systems (Ph) providing much lower solubility than the Cy analogs. This can be attributed to the more favorable formation of intermolecular aggregates, most likely caused by π-stacking. These effects are more explicit in the *para*-substituted hosts, where the solubility becomes more challenging, to a point at which the formed aggregates of **AB-pTTA-(1,3)Ph** could not be dissolved in any chosen organic solvent. To deal with this obstacle, the host structure was further altered by incorporating additional tags such as *n*-octyl (O) and triethylene glycol (T), which were chosen due to their known ability to enhance solubility in organic solvents.[31] The introduction of octyl chains unfortunately did not enhance the solubility but rather decreased it. This is especially apparent for the host **AB-O-mTTA-(1,3)Ph**, which featured too low solubility for NMR-titrations in acetone-d_6 and was thus measured in DCM-d_2 (see the SI). In contrast, the introduction of a T-tag (**AB-mTTA-(1,3)PhT**) slightly increased the solubility. NMR-titrations of the tagged hosts generally revealed a decrease in the binding constant (Fig. 4), which led us to refrain from their further investigation.

All of the above binding studies were performed on the photostationary state (PSS) after blue or UV irradiation,

respectively, which contains a minor component of the respective other isomer. The respective *E*/*Z* ratios are given in Table S7. Investigating *K* in a mixture of *E* and *Z* isomers could lead to errors, as the minor isomer may shift the binding equilibrium of the major isomer due to its deviating binding constant. We therefore made a comparative analysis of both the respective major and minor isomers for the host with the largest isomeric contrast in *K*, *i.e.* **AB-mTTA-Cy**. Fig. S31 in the SI shows the spectra after blue or UV irradiation, respectively, with the resonances of the major and minor resonances assigned. The resulting *E*/*Z* ratio in the PSS is given in Table S5 for this host and all other hosts. Based on the spectral assignment, the binding constant was analyzed separately for each isomer as a major or a minor component; see Fig. S26 and the accompanying explanation in the SI. The resulting anion binding constant of the minor component deviates around 10% from the anion binding constant in the major case, remaining within the error margin. Therefore, our anion binding constants can be considered reliable.

We then turned our attention to the variation of the photoswitchable motif for the host frameworks that previously exhibited the highest binding constants or the most significant differences in the binding properties of the *E*/*Z*-isomers. We conducted this by exchanging the central AB unit with an AAP motif, while maintaining a *meta*-substitution pattern. When employing a host with a cyclohexyl linkage between the triazole rings (**AAP-mTTA-Cy**), a slight increase in the binding constant of the *Z*-isomer was noticed ($\log(K_Z/M^{-1})$ = 3.4). Conversely, the host with a phenyl linkage (**AAP-mTTA-(1,3)Ph**) shows more distinct differences ($\log(K_Z/M^{-1})$ = 3.9 *vs.* $\log(K_E/M^{-1})$ = 2.6). Although these AAP-*Z*-isomers bind anions slightly less effectively than their parent AB-host, the *E*-isomers display significantly weaker binding to the anion, resulting in a combination of strong anion binding with markedly different binding properties of the two isomers, eliminating the need for a chiral structure as required for the parent AB hosts. By introducing an AAP unit, an additional pyrazole ring is inserted into the host's framework, which increases the distance between the triazole protons and might prevent the formation of a suitable cavity in the *E*-isomer.

DFT calculations

In order to shed some light onto the conformations of the *E*/*Z*-isomers that are likely to contribute to anion binding, DFT calculations were conducted exemplarily for the strongly binding **AB-mTTA-(1,3)Ph** (Fig. 5). The binding energies for both isomers were determined from geometry optimizations of the host structures with and without a chloride anion. Upon examining the optimized structures binding a chloride anion, it becomes apparent that the binding energy heavily relies on the linker and switching unit. In the presence of a (1,3)Ph linker, the respective lowest energy (according to the adopted DFT/PCM model, see the SI, section 2 'DFT' and Tables S3–S6 for details) *E*-isomer adopts a helicene-like conformation due to cooperative effects of the aromatic rings, thus resulting in a favorable cavity for the chloride anion (Fig. 5a). In contrast,

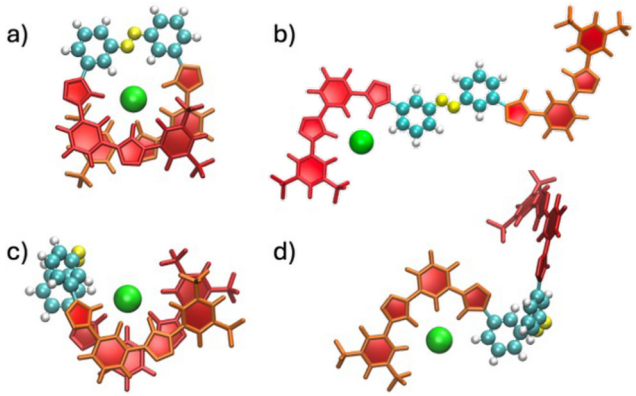

Fig. 5 Lowest energy conformers of **AB-mTTA-(1,3)Ph** bound to chloride calculated using DFT for the *E* isomer ((a), (b)) and the *Z* isomer ((c), (d)).

the lowest energy *Z*-isomer has a tub-like geometry, facilitating the coordination of a chloride guest by the triazole protons from one half-space, leaving the other half-space open to access (Fig. 5b).

Taking into account that the inclusion of dispersion corrections, the implicit solvent representation, and the neglect of conformational entropy artificially favors folded conformations, it appears plausible to also consider open, *i.e.* unfolded, conformers. As a matter of fact, the open structures shown in Fig. 5(c and d) are predicted to be nearly degenerate with the folded structures by standard non-dispersion corrected DFT (see Tables S3–S6). Indeed, an equilibrium between open and folded conformers has previously been reported for a similar system.[11] This naturally explains why the experimentally observed binding constants are nearly equal for both isomers (Fig. 4; $\log(K_E/M^{-1})$ = 4.2 and $\log(K_Z/M^{-1})$ = 4.3). The corresponding theoretical numbers for the open structures are 6.2 (3.0) and 5.9 (3.1) with (without) dispersion corrections.

Back-isomerization

Building up on the stronger anion affinity of the *Z*-isomers, we finally investigated the influence of guest presence on the photo-isomerization and thermal back relaxation. UV-vis spectroscopy was employed to quantify the thermal back-isomerization of a selected host structure (Fig. 6). The addition of TBACl significantly reduces the thermal relaxation rate of the *Z*-isomer by a rate reduction of a factor of about two. We attribute this to *Z* isomer stabilization upon the formation of a host–guest complex in the presence of salt. Thus, the thermal back-isomerization rate is demonstrated to be dependent on the presence of anions.

We further explored this phenomenon with respect to photoisomerization with three representative hosts (**AB-mTTA-Cy**, **AB-mTTA-(1,3)Ph** and **AAP-mTTA-(1,3)Ph**), by monitoring the response of *Z*-isomers to short light pulses, employing blue (AB) or green (AAP) light, respectively (Fig. 7a). It was observed that the photo-induced back-isomerization was also

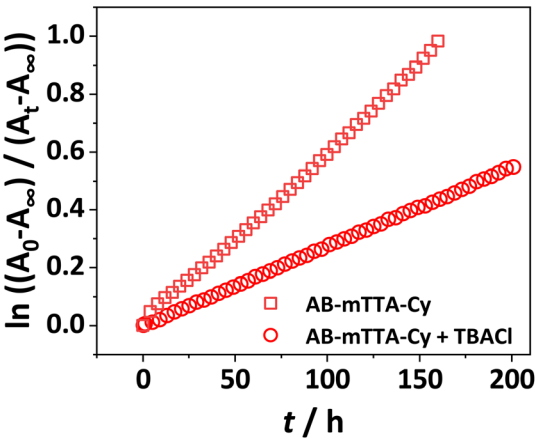

Fig. 6 UV-vis spectroscopy study of the buildup of the *E*-isomer by thermal relaxation of *Z*-**AB-mTTA-Cy** (50 μM, $CHCl_3$), monitored using *E*-isomer absorbance A_t.

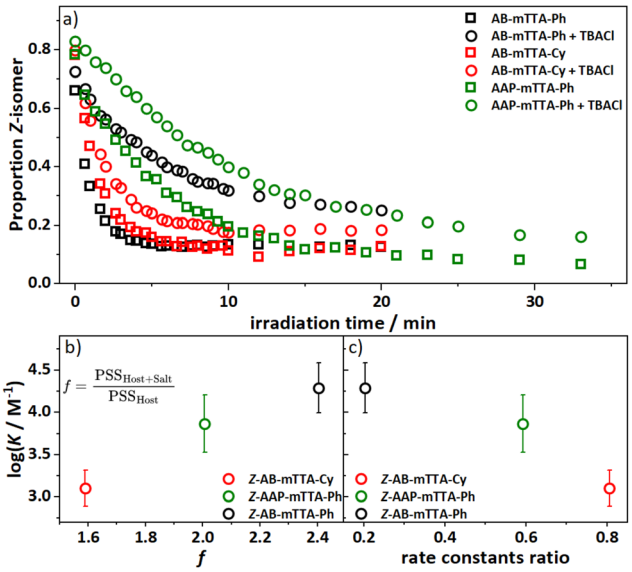

Fig. 7 (a) Photoisomerization of the *Z*-isomers of **AB-mTTA-Cy**, **AB-mTTA-(1,3)Ph** and **AAP-mTTA-(1,3)Ph** (1 mM) upon blue (AB, 435 nm) or green (AAP, 520 nm) light irradiation in acetone-d_6 with and without the addition of TBACl (10 equivalents). Plots of *K* concerning the *Z*-isomer of the respective host with chloride against (b) the fraction *f* calculated from the PSS with and without salt and (c) the ratio of the photoisomerization rate constants.

clearly modified in the presence of TBACl. On the one hand, salt addition decreases the rate of back-isomerization of the *Z*-isomer, which can be analyzed from the initial slope r_0 from Fig. 7a. On the other hand, the presence of salt also leads to an altered photostationary state, as evident from different plateau values f_Z at long irradiation times. It should be noted that the attainment of the PSS also depends on the power of the light source and the absorption of the host at its wavelength. Therefore, the lower rate for the AAP host may partly result from the lower power of the utilized green LED, compared to the blue laser used for the AB hosts. Therefore, the anion-tunability of the back-isomerization of the different hosts cannot be directly compared from these raw data. To compensate for the above influences, we therefore analyzed the ratio of initial isomerization rates $r = r_0^{salt}/r_0^{nosalt}$, whereby we found that this ratio clearly correlates with the binding constant (Fig. 7c, and numbers given in Table S8). A higher binding constant reduces the efficiency of back-isomerization to the *E* state, as the *Z* isomer becomes stabilized due to anion binding. In comparison with the anion influence on thermal back-isomerization, where the back-isomerization rate changed by a facor of 0.5, the contrast in photo-isomerization is less pronounced (r = 0.8 for *Z*-**AB-mTTA-Cy**). This difference is probably due to different isomerization pathways.

Similar to the isomerization rate, the ratio of the *Z* isomer fraction in the PSS, $f = f_Z^{salt}/f_Z^{nosalt}$, is found to depend on the binding constant (Fig. 7b, and numbers given in Table S8). As the binding constant increases, the salt effect on the PSS rises, indicating that it is indeed the strong anion binding which is shifting the PSS further to the *Z* side. The equilibrium between the *E*/*Z*-isomers and the isomerization rates are thus affected by the availability of anions.

It is interesting to shed light on the photophysical properties which influence the photoisomerization rate and the PSS, as several mechanisms might be involved: anion binding might modify the host absorbance or the quantum yield of photoconversion, or it might even more generally modify the pathway of photoconversion. To elucidate the mechanisms, we performed additional absorption and fluorescence studies on the dependence on anion availability. The absorbance spectra of all three hosts with and without bound anions showed no significant differences (see the SI, Fig. S30), such that the absorbance difference can be ruled out as the origin of anion-dependent photoisomerization. Subsequently, the fluorescence quenching of the three hosts by anions (0 to 10 equivalents TBACl) was studied, revealing an unexpected up to 10% enhancement of fluorescence (see the SI, Fig. S31 and Table S9). This fluorescence enhancement in the presence of anions might be the result of an interception of the excited state energy, decreasing the efficacy of the photoswitch intrinsic photoisomerization pathways and directing it to fluorescence. However, this effect cannot quantitatively account for the observed rate constant reduction, which amounts to 20% to 80%. We can thus conclude that only a small fraction of the reduction of isomerization efficiency is channeled into fluorescence. Probably more complex modifications of the photophysical pathways following excitation are responsible for the dependence of the PSS and isomerization rate on the presence of anions.

With these findings, we have proven the concept of Fig. 1, as isomerization and anion binding equilibria mutually influence each other: the state of isomerization determines the anion binding equilibrium, while anion binding in turn modifies the equilibrium of the isomers.

Further tuning these mutual influences will form the basis for optimizing photosystems that control as well as react to anion availability.

Conclusions

In conclusion, a systematic investigation using *in situ* NMR titrations on the influence of the structural motifs, including switching units, linkers and solubility tag-chains, of a new family of light-switchable anion binding oligo-triazole-based host molecules bearing a central switching unit was performed. For AB-based hosts, the presence of a *trans*-1,2-cyclohexane linker is beneficial for achieving a contrast between the binding constants of the isomers, while an aromatic 1,3-linkage led to higher binding constants with no isomer differentiation. In contrast, incorporation of an AAP switching unit led to an improved divergence in the binding affinities of the *Z- vs. E*-isomer by forming distinct anion binding cavities with an increased distance between the triazole rings. This enables the formation of a more suitable cavity in the *Z*-isomer. In addition, the use of an AAP switching unit also led to an improved PSS ratio, *i.e.* a lower fraction of the respective minor isomeric component, and enhanced solubility.

Ultimately, the observed differences in anion binding strength are sufficient to enable an anion-dependent $Z \rightarrow E$ back-isomerization of the systems, as in the presence of a salt, thermal and photoinduced back-isomerization are less efficient. We proposed that this dependency is based on stabilization of the *Z*-isomer by host–guest complex formation, although additional anion-induced changes in the photophysical isomerization mechanisms cannot be ruled out. The isomerization rate constants and the photostationary state both correlate well with the anion binding constant of the *Z*-isomer. These properties, in combination with the host variability by selecting appropriate structural motifs, are an interesting basis for further optimization of anion-binding photosystems. Along this line, we will in the future apply these hosts in supramolecular gels with the goal of developing adaptively reacting photosystems.

Experimental

Materials for binding studies

Acetone-d_6 (99.9%), dichloromethane-d_2 (99.9%), tetrabutylammonium chloride (TBACl, 99.0%), tetrabutylammonium benzoate (TBAB, 99.0%) and tetrabutylammonium acetate (TBAAc, 97%) were all purchased from Sigma Aldrich (Germany). Acetone-d_6 and dichloromethane-d_2 were dried using molecular sieves (3 Å, AppliChem, Germany) for at least 24 hours. TBACl, TBA benzoate (TBAB) and TBA acetate (TBAAc) were dried in a high vacuum at 50 °C overnight. All preparational work was done under an argon atmosphere to avoid moisture.

NMR titrations

The NMR titrations were carried out with a constant concentration of the host (1 mM) and varying amounts of salt (0 to 10 equiv.) dissolved in acetone-d_6, if not stated otherwise. The samples were filled into 5 mm precision NMR tubes and sealed with a laboratory film to prevent evaporation and were irradiated for at least 20 min prior to measurement with either a 365 nm UV light-emitting diode (LED) with a flux of 20.8 mW cm^{-2}, a green LED with a flux of 19.2 mW cm^{-2} or a 447 nm blue laser with a flux of 280 mW cm^{-2}. ^{1}H NMR spectra were recorded on a Bruker Avance III HD 400 MHz NMR spectrometer equipped with a gradient probe head with a selective ^{1}H insert ("Diff50", Bruker). A temperature of 25 °C was ensured by insertion of a reference tube containing a PT100 thermocouple in oil prior to experiments.

In situ NMR experiments with irradiation

For *in situ* NMR experiments with light irradiation using LEDs, 5 mm precision NMR tubes were filled with 300 µL of the sample solution (1 mM), followed by insertion of the end of an optical fiber waveguide into the NMR tubes. A schematic of the setup is shown in Scheme S28. It allows alternating irradiation as well as irradiation during measurement for unstable isomers with UV (365 nm, 20.8 mW cm^{-2}) and blue (447 nm, 280 mW cm^{-2}) light. For photoisomerization studies of the $Z \rightarrow E$ transition, the samples underwent prior UV irradiation for 2 hours. Subsequently, the samples were irradiated with a pulse of blue light (447 nm, 280 mW cm^{-2}) for a few seconds before ^{1}H-NMR measurement. This process was repeated until reaching a plateau for the proportion of the *Z* state.

Author contributions

L. Hoppmann and L.-M. Entgelmeier designed, synthesized and analyzed the host systems, L. Wyszynski and P. Steinforth carried out the *in situ* photochemical switching, anion-binding and back-isomerization studies, and M. Böckmann and N. Doltsinis performed the computational studies. O. García Mancheño and M. Schönhoff designed and supervised the work. All authors contributed to the interpretation of data and preparation of the manuscript.

Conflicts of interest

There are no conflicts to declare.

Data availability

The data supporting this article have been included as part of the supplementary information (SI). Supplementary information: NMR titrations, UV-vis and computational studies, synthetic procedures, analytical data and NMR spectra of the new compounds (PDF). See DOI: https://doi.org/10.1039/d5ob01664a.

Acknowledgements

This work was funded by the Deutsche Forschungsgemeinschaft (DFG, German Research Foundation) within the SFB 1459 – project ID 433682494, and the NMR spectrometer was funded by the DFG *via* proposal INST 211/999-1 FUGG, project ID 452849940.

References

1 (*a*) K. Maslowska-Jarzyna, E. York, E. Feo, R. M. Maklad, G. Bao, M. Fares and P. A. Gale, *Chem*, 2025, **11**, 102695; (*b*) D. A. McNaughton, W. G. Ryder, A. M. Gilchrist, P. Wang, M. Fares, X. Wu and P. A. Gale, *Chem*, 2023, **9**, 3045–3112; (*c*) N. Busschaert, C. Caltagirone, W. van Rossom and P. A. Gale, *Chem. Rev.*, 2015, **115**, 8038–8155; (*d*) P. A. Gale and W. Dehaen, *Anion Recognition in Supramolecular Chemistry*, Springer, 2011.

2 N. H. Evans and P. D. Beer, *Angew. Chem., Int. Ed.*, 2014, **53**, 11716–11754.

3 (*a*) P. A. Gale and C. Caltagirone, *Chem. Soc. Rev.*, 2015, **44**, 4212–4227; (*b*) *Anion Sensing*, ed. I. Stibor, Springer Berlin Heidelberg, Berlin, Heidelberg, 2005, vol. 255.

4 B. A. Moyer, L. H. Delmau, C. J. Fowler, A. Ruas, D. A. Bostick, J. L. Sessler, E. Katayev, G. Dan Pantos, J. M. Llinares, M. A. Hossain, S. O. Kang and K. Bowman-James, in *Template Effects and Molecular Organization*, Elsevier, 2006, vol. 59, pp. 175–204.

5 P. A. Gale, J. T. Davis and R. Quesada, *Chem. Soc. Rev.*, 2017, **46**, 2497–2519.

6 *Anion-binding catalysis*, ed. O. García Mancheño, Wiley-VCH, Weinheim, Germany, 2022.

7 (*a*) J. de Jong, J. E. Bos and S. J. Wezenberg, *Chem. Rev.*, 2023, **123**, 8530–8574; (*b*) Z. Kokan and M. J. Chmielewski, *J. Am. Chem. Soc.*, 2018, **140**, 16010–16014; (*c*) P. A. Gale, E. N. Howe and X. Wu, *Chem*, 2016, **1**, 351–422; (*d*) L. Chen, S. N. Berry, X. Wu, E. N. Howe and P. A. Gale, *Chem*, 2020, **6**, 61–141; (*e*) S. Lv, X. Li, L. Yang, X. Wang, J. Zhang, G. Zhang and J. Jiang, *J. Phys. Chem. A*, 2020, **124**, 9692–9697.

8 A. Lutolli and A. H. Flood, in *Molecular Photoswitches*, ed. Z. L. Pianowski, Wiley, 2022, pp. 541–563.

9 S. Lee and A. H. Flood, *J. Phys. Org. Chem.*, 2013, **26**, 79–86.

10 (*a*) D.-H. Qu, Q.-C. Wang, Q.-W. Zhang, X. Ma and H. Tian, *Chem. Rev.*, 2015, **115**, 7543–7588; (*b*) L. E. Bickerton, T. G. Johnson, A. Kerckhoffs and M. J. Langton, *Chem. Sci.*, 2021, **12**, 11252–11274.

11 S. Shinkai, T. Nakaji, Y. Nishida, T. Ogawa and O. Manabe, *J. Am. Chem. Soc.*, 1980, **102**, 5860–5865.

12 (*a*) G. M. Walker, *Crit. Rev. Biotechnol.*, 1994, **14**, 311–354; (*b*) X. Shi, H. Xiao, X. Chen and K. S. Lackner, *Chem. – Eur. J.*, 2016, **22**, 18326–18330; (*c*) E. R. Orhue and U. O. Frank, *J. Appl. Nat. Sci.*, 2011, **3**, 131–138.

13 K. Dąbrowa, P. Niedbała and J. Jurczak, *Chem. Commun.*, 2014, **50**, 15748–15751.

14 V. Haridas, S. Sahu, P. P. P. Kumar and A. R. Sapala, *RSC Adv.*, 2012, **2**, 12594–12605.

15 Y. Wang, F. Bie and H. Jiang, *Org. Lett.*, 2010, **12**, 3630–3633.

16 Y. Hua and A. H. Flood, *J. Am. Chem. Soc.*, 2010, **132**, 12838–12840.

17 Y. Hua, Y. Liu, C.-H. Chen and A. H. Flood, *J. Am. Chem. Soc.*, 2013, **135**, 14401–14412.

18 S. Lee, Y. Hua and A. H. Flood, *J. Org. Chem.*, 2014, **79**, 8383–8396.

19 F. C. Parks, Y. Liu, S. Debnath, S. R. Stutsman, K. Raghavachari and A. H. Flood, *J. Am. Chem. Soc.*, 2018, **140**, 17711–17723.

20 (*a*) S. Grewal, S. Roy, H. Kumar, M. Saraswat, N. K. Bari, S. Sinha and S. Venkataramani, *Catal. Sci. Technol.*, 2020, **10**, 7027–7033; (*b*) S. A. Rahaman, M. S. Hossain, S. Baburaj, A. Biswas, A. Bag and S. Bandyopadhyay, *Org. Biomol. Chem.*, 2019, **17**, 5153–5160; (*c*) A. Docker, X. Shang, D. Yuan, H. Kuhn, Z. Zhang, J. J. Davis, P. D. Beer and M. J. Langton, *Angew. Chem., Int. Ed.*, 2021, **60**, 19442–19450.

21 A. Kerckhoffs, I. Moss and M. J. Langton, *Chem. Commun.*, 2022, **59**, 51–54.

22 Q. Jin, Y. Hai, L.-J. Liu, T.-G. Zhan and K.-D. Zhang, *Org. Chem. Front.*, 2025, **12**, 1217–1226.

23 C. Wang, K. Ye, Z. Yan, S. Ma, J. Fan and C. Bao, *Sci. China: Chem.*, 2025, **68**, 3602–3610.

24 H.-Y. Duan, S.-T. Han, T.-G. Zhan, L.-J. Liu and K.-D. Zhang, *Angew. Chem., Int. Ed.*, 2023, **62**, e202212707.

25 (*a*) S. J. Wezenberg, *Chem. Commun.*, 2022, **58**, 11045–11058; (*b*) P. Tecilla and D. Bonifazi, *ChemistryOpen*, 2020, **9**, 529–544; (*c*) C.-T. Poon, W. H. Lam and V. W.-W. Yam, *J. Am. Chem. Soc.*, 2011, **133**, 19622–19625; (*d*) M. Lohse, K. Nowosinski, N. L. Traulsen, A. J. Achazi, L. K. S. von Krbek, B. Paulus, C. A. Schalley and S. Hecht, *Chem. Commun.*, 2015, **51**, 9777–9780; (*e*) K. Dąbrowa, P. Niedbała and J. Jurczak, *J. Org. Chem.*, 2016, **81**, 3576–3584; (*f*) K. Dąbrowa and J. Jurczak, *Org. Lett.*, 2017, **19**, 1378–1381.

26 (*a*) H.-S. Tang, N. Zhu and V. W.-W. Yam, *Organometallics*, 2007, **26**, 22–25; (*b*) M. Yamamura, Y. Okazaki and T. Nabeshima, *Chem. Commun.*, 2012, **48**, 5724–5726.

27 C. E. Weston, R. D. Richardson, P. R. Haycock, A. J. P. White and M. J. Fuchter, *J. Am. Chem. Soc.*, 2014, **136**, 11878–11881.

28 M. Zurro, S. Asmus, S. Beckendorf, C. Mück-Lichtenfeld and O. García Mancheño, *J. Am. Chem. Soc.*, 2014, **136**, 13999–14002.

29 D. G. Piekarski, P. Steinforth, M. Gómez-Martínez, J. Bamberger, F. Ostler, M. Schönhoff and O. García Mancheño, *Chem. – Eur. J.*, 2020, **26**, 17598–17603.

30 P. Steinforth, M. Gómez-Martínez, L.-M. Entgelmeier, O. García Mancheño and M. Schönhoff, *J. Phys. Chem. B*, 2022, **126**, 10156–10163.

31 (*a*) M. Giese and M. Albrecht, *ChemPlusChem*, 2020, **85**, 715–724; (*b*) T. Shimada, Y. Watanabe, T. Kajitani, M. Takeuchi, Y. Wakayama and K. Sugiyasu, *Chem. Sci.*, 2023, **14**, 822–826; (*c*) T. F. A. de Greef, M. M. L. Nieuwenhuizen, P. J. M. Stals, C. F. C. Fitié, A. R. A. Palmans, R. P. Sijbesma and E. W. Meijer, *Chem. Commun.*, 2008, 4306–4308.